NANO LETTERS

xxxx
Vol. 0, No. 0
A−F

Gradient Chemical Micropatterns: A Reference Substrate for Surface Nanometrology†

Duangrut Julthongpiput,‡ Michael J. Fasolka,*,‡ Wenhua Zhang,‡ Tinh Nguyen,§ and Eric J. Amis‡

Polymers Division and Materials and Construction Research Division, National Institute of Standards and Technology, Gaithersburg, Maryland 20899

Received March 31, 2005; Revised Manuscript Received June 14, 2005

ABSTRACT

We present fabrication routes for a new type of surface specimen that exhibits a micropattern with a gradient in chemical contrast between the pattern domains. Design elements in the specimen allow chemical contrast in the micropattern to be related to well-established surface characterization data, such as contact angle measurements. These gradient specimens represent a reference tool for calibrating image contrast in chemically sensitive scanning probe microscopy techniques and a platform for the high-throughput analysis of polymer thin film behavior.

Substrate surface chemistry is a governing factor in thin film materials behavior, polymer self-assembly, adhesion and wetting, friction, and biocompatibility. As such, surface chemistry, or surface energy, is an increasingly important engineering parameter in a variety of materials systems and technologies, including nanolithography masks,[1−3] MEMS and NEMS,[4,5] microfluidics,[6,7] and tissue scaffolds.[8,9] Moreover, with the advent of soft-lithography techniques,[10,11] a growing number of studies demonstrate that micrometer- and nanometer-scale patterns in surface chemistry affect, and sometimes enhance, the structure and properties of systems deposited upon them.[12−15] In addition, surface chemistry is recognized, but often underevaluated, as a factor that contributes to the contrast of nanoscale micrographs generated by both common and emerging scanning probe microscopy (SPM) techniques, including atomic force microscopy, friction force microscopy, chemical force microscopy, and atomic force acoustic microscopy (AFM, FFM, CFM, and AFAM, respectively).

There are many techniques to impart tailored surface energy and chemical patterns on a variety of substrate materials. Most of these methods allow only "single-case" studies because they result in specimens that exhibit a particular chemistry, or in the case of soft lithography, an alternating pattern of two chemistries. In contrast, multivariate or "combinatorial" fabrication approaches, which result in specimens that exhibit many cases on a single substrate, present a considerable advantage because they enable the rapid and thorough analysis of the effect of surface chemistry over a wide range. In this regard, published works[16−19] demonstrate the ability to create continuous surface energy *gradients*, and a growing body of research illustrates the utility of these multivariate substrates for mapping the effect of surface energy on phenomena such as wetting[20−22] and self-assembly.[23]

In this paper, we discuss the fabrication and utility of a new class of substrates that combines a microscale chemical pattern with a surface energy gradient. These specimens exhibit micropatterns that gradually and systematically change in their *chemical contrast,* that is, the surface energy differences between surface domains, and thereby present a multitude of pattern conditions on a single substrate. By design, our gradient substrates allow for the chemical contrast along the micropattern to be calibrated with well-understood characterization techniques such as contact angle measurements or surface spectroscopy. Moreover, to produce these specimens we have developed a promising new method for patterning monochlorosilane (MCS) self-assembled monolayers (SAMs) that combines microcontact printing and vapor deposition. This method provides reproducible, high-quality, microscale SAM patterns on *silicon substrates* in a way that is amenable to multisample batch processing.

Primarily, we intend our gradient micropattern ($\nabla\mu$p) specimens to serve as reference substrates useful for the development and calibration of surface-chemistry-sensitive SPM techniques such as CFM, FFM, and AFAM. As will be seen below, $\nabla\mu$p reference substrates provide a means to calibrate image contrast with respect to "traditional" chemical measures and allow for probe characterization, especially for

† Contribution of the National Institute of Standards and Technology.
* Corresponding author. E-mail mfasolka@nist.gov.
‡ Polymers Division.
§ Materials and Construction Research Division.

10.1021/nl050612n CCC: $30.25 © xxxx American Chemical Society PAGE EST: 5.8
Published on Web 00/00/0000

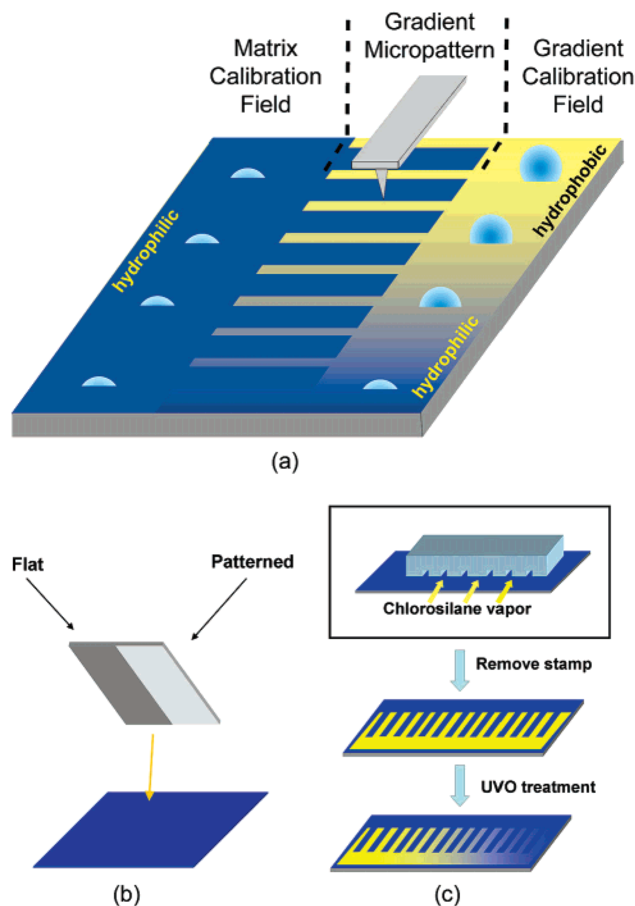

Figure 1. (a) Schematic illustration of ∇μp specimen design. The central part of the specimen has a pattern of micrometer-scale lines that gradually change in their chemistry (e.g., surface energy) with respect to a surrounding matrix, which exhibits a fixed surface energy. Scheme for preparing a ∇μp using vapor deposition of ODS on a SiO_2 substrate: (b) Illustration of a composite elastomer stamp, which has both flat and corrugated regions. (c) Illustration of vapor-mediated soft lithography and gradient UVO exposure.

cases (e.g., CFM) where the quality of tip functionalization is important. In addition, these specimens hold promise as screening tools for the high-throughput analysis of thin film phenomena. In this letter, we demonstrate both of these capabilities through illustrative case studies.

Figure 1 illustrates our ∇μp specimen design schematically. The central part of the reference specimen has a pattern of micrometer-scale lines that gradually change in their chemistry (e.g., surface energy) with respect to a surrounding matrix, which exhibits a fixed surface energy. This patterned region is the experiment platform. For example, in the case of SPM calibration, images acquired along the patterned region generate a series of micrographs with gradually changing contrast. Wide "calibration" fields, which bound the patterned area, directly reflect the changing chemistry of the lines and the static chemistry of the matrix. This is an important aspect of the specimen design because well-understood measurements (e.g., contact angle) along the calibration fields can be used to determine chemical differences in the ∇μp, which are difficult to gauge. Such calibration enables quantitative correlation between chemical contrast and experiments conducted on the patterned area. Thus, for our example of SPM micrographs, the specimen relates the image contrast to the calibration measurements.

Specimen Fabrication and Validation. Fabrication of ∇μp specimens involves soft-lithography of appropriate SAM molecules onto a planar substrate followed by a graded processing step that modulates the chemical contrast. The key to creating the specimen design shown in Figure 1a is a composite elastomer stamp, which has both flat and corrugated regions, as shown in Figure 1b. Such a stamp allows us to deposit a SAM layer consisting of a micropatterned strip with an adjacent solid calibration field (Figure 1c). Next, a graded UV-ozonolysis (UVO), applied along the specimen, gradually modifies the chemistry of the patterned SAM (and calibration field) along one direction. During this UVO processing, methyl-terminated alkyl chain monolayers (hydrophobic) are converted into carboxylic acid terminated (hydrophilic) chains.[24] As UVO exposure time is varied along the length of the specimen, the density of hydrophobic-ended molecules decreases, whereas the density of the hydrophilic-ended chains increases. As we demonstrated previously,[25] established wet microcontact printing techniques[11,13,26] can be used to produce ∇μp specimens consisting of alkanethiol SAMS on Au substrates. Although this represents an easy procedure for fabricating a ∇μp, problems associated with traditional thiol SAM printing with respect to reproducibility and stability are well known. In particular, the surface coverage of wet-printed SAM depends on a variety of factors, including the contact time and pressure and ink concentration. In addition, the alkanethiol SAM patterns are not stable over long periods in ambient conditions or at elevated temperatures.[19] These effects make thiol printing an inadequate route for producing specimens appropriate for use as references or for thin film studies that require higher temperature processing.

To improve the vigor and versatility of our specimens, we developed a new method for preparing chlorosilane, that is, *n*-octyldimethylchlorosilane (ODS), SAM patterns on (oxide terminated) silicon surfaces by combining microcontact printing and vapor deposition methods. As illustrated in Figure 1c, in this new technique the composite elastomer stamp is sectioned so that the edge of the corrugated area is exposed. Application of such a stamp to the substrate physically masks selected areas of the substrate and creates a series of microchannels over the substrate surface (see Figure 1c, top). Accordingly, when the stamp/substrate system is immersed in a saturated ODS vapor, the vapor travels down the microchannels and an ODS SAM is deposited on areas of the substrate not masked by the stamp (Figure 1c, middle). As discussed above, fabrication of the ∇μp specimen is completed by a graded UVO exposure. As verified by previous secondary ion mass spectrometry (SIMS) analysis,[24] UVO treatment adds a range of oxygen-containing functionalities to the ODS layer, including carboxylate, ether, and carbonyl species. Accordingly, the exposure gradient gradually changes the original hydrophobic ODS SAM to a more hydrophilic SAM. (Fabrication details, including stamp preparation and notes on specimen lifetime, can be found in the Supporting Information.)

Vapor-deposited chlorosilane SAMs on silicon are more robust than thiol SAMs on gold, resulting in ∇μp substrates that can be stored, cleaned, reused, and processed at higher temperatures. Moreover, previous X-ray reflectivity analysis[24] and our ellipsometry (we report a thickness of ∼1 nm) and water contact angle measurements (we found 96 ± 2°) of similarly processed ODS SAM layers confirm a high-quality, near monolayer coverage of the substrate, with the height of the layer close to that expected from a fully packed and stretched ODS SAM (∼1.2 nm). Indeed, in a comparison of common deposition techniques, McCarthy et al.[27−29] report that the highest quality SAMs were obtained using a vapor phase reaction. Furthermore, the vapor deposition process reduces solvent and chlorosilane waste and minimizes the deposition of aggregated organosilane molecules because this species is rarely vaporized.[30] Perhaps most importantly, *the vapor-patterning process allows many specimens to be processed simultaneously under identical conditions*. Although we have not explored the prospect, it may be possible to use this technique to make submicron-scale chemical patterns. Because our technique relies upon the ability of ODS molecules to travel into and along the microchannels, we expect that this will necessitate the fabrication of a stamp with high-aspect ratio corrugations, that is, a stamp that forms channels with a cross section large enough to accommodate vapor diffusion. One challenge here is that high-aspect ratio elastomer corrugations can be prone to collapse when applied to a substrate.

It is important to verify that the chemistries exhibited (and measured) along the calibration fields are reflected in the patterned area in order to validate the specimen design. Such verification was achieved by conducting contact angle measurements along the length of the ∇μp specimen and along each calibration field. Figure 2a shows water contact angle (hereafter "contact angle") measurements collected along a representative specimen subjected to a linear UVO exposure gradient ranging from 0 to 80 s. Along the matrix field, contact angles (θ_A) remain constant (∼21°), whereas the contact angles on the gradient calibration field (θ_B) decrease from approximately 98 to 21°. Water contact angle measurements along the gradient micropattern (θ_P) varied from 68 to 16°. To illustrate chemical congruence between calibration fields and the patterned area, model contact angle values (θ_M) were calculated according to equation 1[31]

$$\frac{1}{(\theta_M)} = \frac{\phi_A}{(\theta_A)} + \frac{\phi_B}{(\theta_B)} \quad (1)$$

In this model, ϕ_A and ϕ_B reflect the relative surface areas of the matrix (SiO_2) and gradient (graded SAM) in the patterned area, respectively. In our current example, the nominal matrix/gradient surface area ratio is 1:5. As can be seen in Figure 2a, measured θ_P values agree well with the θ_M predictions, indicating that the chemistry of the patterned domains reflects the constituent chemistry in the calibration fields. However, this simple model does not capture the effect of the micropattern on the wetting behavior of droplets; the fact that θ_P is observed to be slightly lower than θ_M is

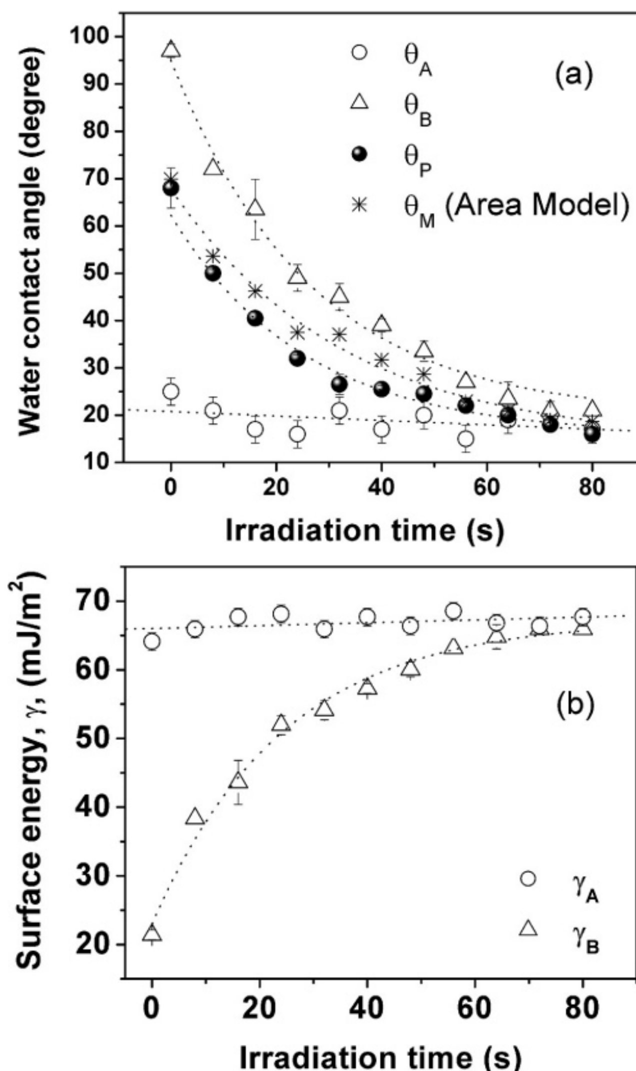

Figure 2. Validation and calibration of the ∇μp. (a) Measured water contact angles and (b) calculated (see text) surface energies along a representative ∇μp specimen.

hypothesized to be due to such effects.[32] Indeed, although it is not the focus of this paper, ∇μp specimens would provide a means to study such phenomenon. Also, this model does not reflect the contribution that surface roughness would make to the observed contact angles. However, for our system such effects are minimal because the RMS roughness of both the silicon wafer substrates we employ and the overlying SAMs are well below 1 nm, as established by AFM.

For our specimens, the surface energy (γ) was estimated by the Good and Girifalco geometric mean approximation method (GMA method),[33] which employs contact angle measurements of two fluids for which the polar and dispersive components of γ are known. The procedure for estimating γ for UVO-modified ODS surfaces is discussed in detail elsewhere.[24] In our specimens, γ in the gradient calibration field spanned 20−63 mJ/m^2, and the matrix field was approximated to be 63 mJ/m^2, as shown in Figure 2b.

Applications of ∇μp Specimens. The ∇μp specimens are useful for gauging tip quality, for calibrating image contrast, and for determining sensitivity in chemically sensitive SPM

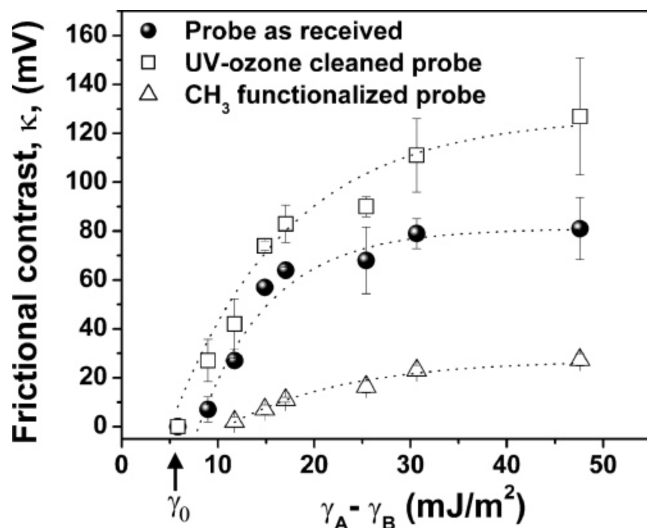

Figure 3. AFM frictional contrast, K, vs surface energy differences ($\gamma_A - \gamma_B$) obtained with probes of different chemical quality on $\nabla\mu$p specimen. γ_0 marks the minimum γ-difference detectable by a particular probe.

techniques such as CFM. To demonstrate this, we used a $\nabla\mu$p specimen to calibrate a series of "friction" (i.e., lateral force) AFM measurements acquired with probes of different chemical quality. Images were acquired according to procedures described in detail elsewhere[34−36] and according to procedures detailed in the Supporting Information section. For contrast calibration, we employ a friction contrast factor (K), which represents the differential lateral cantilever deflection measured between ODS and SiO_2. All of the images were acquired using the same cantilever probe and with an applied normal force of approximately 350 nN, as estimated from force−distance measurements, the setpoint deflection, and the nominal cantilever stiffness, 0.06 nN/m (see the Supporting Information for details). K is extracted from raw lateral force AFM data processed through the common $^1/_2|C_{\mathrm{trace}} - C_{\mathrm{retrace}}|$ relation, where C_{trace} (C_{retrace}) is the deflection for points along the "trace" ("retrace") fast-scan direction.[37,38] K values were averaged along the slow scan direction (average "cross section") and subsequently over several (3−6) micrographs collected at identical contrast ($\gamma_A-\gamma_B$) conditions. For AFM micrographs acquired along the gradient micropattern, K reduces as the UVO irradiation time increases and the pattern domains become more chemically similar. By correlating the position of the micrographs with surface energy measurements along the calibration field, we can calibrate K with respect to γ differences between the gradient and matrix ($\gamma_A - \gamma_B$), as demonstrated in Figure 3. Note that the $\nabla\mu$p specimen gives an entire spectrum of calibration relationships, as opposed to the single calibration relationship given by a traditional specimen.

In addition, the gradient micropattern specimen serves as a tool for comparing the quality of tip functionalization. Figure 3 demonstrates calibration curves for friction contrast versus γ differences collected using three different probe chemistries: (1) a probe as received from the manufacturer, (2) the *same* probe cleaned with UVO, and (3) the *same* probe functionalized with ODS (CH_3 end group). The AFM friction measurements were performed using the *same probe* and identical scanning conditions for direct comparison, as discussed above, and as detailed in the Supporting Information. From the curves shown in Figure 3, it is clear that the friction sensitivity of the probe is enhanced with UVO treatment as compared to the "as received" probe. Conversely, for the CH_3 functionalized probe, K is reduced over the entire range of γ differences. These trends are expected because it is known that UVO treatment removes organic residues, which tend to decrease probe/surface interactions, and because alkylsilane (CH_3) functionalization will tend to decrease friction over both the SiO_2 and SAM regions. The remarkable point is that this single specimen allows for these comparisons to be made in a quantitative manner over a wide range of γ. In addition, the curves of Figure 3 illuminate the relative *sensitivity* of the tested probes, that is, the minimum ODS/SAM γ difference (calibrated minimum contrast condition) observed in the AFM images. We evaluate probe sensitivity through a value, γ_0 (see arrow in Figure 3), which represents the γ difference where $K \approx 0$ (no frictional contrast). From the calibration curves, we observe a trend of, $\gamma_{0,\mathrm{uvo}} < \gamma_{0,\mathrm{as\ received}} < \gamma_{0,CH_3}$, where higher γ_0 values correspond to less-sensitive probes.

$\nabla\mu$p specimens also hold potential for the rapid and thorough analysis of thin film phenomenology. To illustrate this, we used $\nabla\mu$p substrates to investigate the wetting stability of polystyrene (PS) films on chemically patterned substrates. Over a single specimen, the $\nabla\mu$p illuminates the effect of pattern γ-contrast on the film morphology. In this study, a 35-nm PS film (nominal Mw = 760 g/mol, Cat no. 32782-4, Aldrich) was spin-coated from a toluene solution (mass fraction of 1%) onto a fresh $\nabla\mu$p specimen.[43] The as-cast film was smooth and uniform as determined by immediate optical inspection. To accelerate dewetting, we annealed the film library overnight at 60 °C, that is, above the glass transition temperature of PS at this molar mass (∼45 °C).[19] Post-annealed film morphologies were measured by a custom-built automated optical microscopy (AOM) platform,[39] which acquired and collated 1900 contiguous OM images spanning the entire specimen. Figure 4 shows four columns (a−d) of contiguous OM micrographs extracted from positions along the film library where the substrate UVO exposure was 10, 40, 50, and 70 s, respectively. To orient the reader, these columns are superposed over an illustration of the $\nabla\mu$p specimen design. As such, the top and bottom sections of each column show data from the matrix calibration region (SiO_2) and the gradient calibration region (ODS SAM), respectively. The middle section of each column is data from the UVO modified $\nabla\mu$p.

Over the calibration regions, the dewetted film exhibits a pattern of droplet polygons, as typified by random nucleation of holes developed by growth and droplet coalescence.[40] As expected, the matrix calibration field shows similar droplet patterns along the specimen (a−d, top), which further validates our specimen design and fabrication. In contrast, on the gradient calibration field (bottom), γ increases from a to d and the films exhibit increasingly larger droplets and

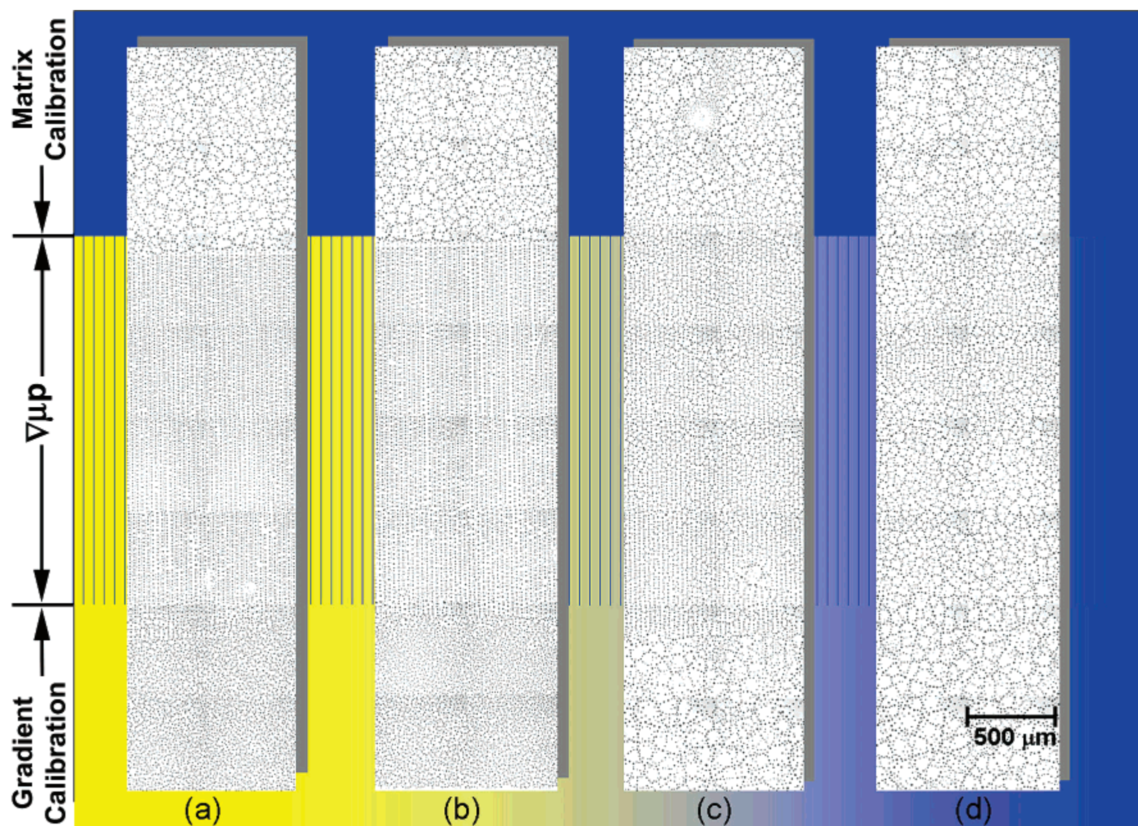

Figure 4. Strips of OM droplet morphology data extracted from the $\nabla\mu$p library. The underlying substrate was irradiated with UVO for (a) 10 s, (b) 40 s, (c) 50 s, and (d) 70 s. PS droplet morphology on matrix calibration field (top), on gradient micropattern (middle), and on gradient calibration field (bottom).

larger polygons. This observation suggests faster hole growth and coalescence kinetics on the higher γ surfaces, which for PS, apparently present a lower barrier to initial hole nucleation and a higher driving force for film instability.[41]

The morphology of droplets over the $\nabla\mu$p (middle) depends on the chemical contrast between the lines and matrix, which decreases from a to d. Regions with strong chemical contrast (a,b) exhibit a *pattern-templated* morphology,[42] characterized by droplets that were distributed evenly along the center of both the high and low γ regions. However, as the γ contrast becomes weaker, the droplets gradually lose registry with the underlying pattern (c), until finally (d) the PS droplets form polygons of the same dimensions seen in each of the calibration fields. In the latter case, γ-differences in the pattern are easily detectable by AFM (Figure 3) and measurements from the calibration fields indicate a γ contrast of $\sim$10 mJ/m^2; yet, dewetting is insensitive to the underlying pattern.

Pattern-directed dewetting behavior is interesting, in part, because it offers means to spontaneously create complex patterns of polymer on a surface. In this light, the data discussed above outline general ranges of γ contrast that result in pattern-templated droplets. However, the data in Figure 4 is only a tiny portion of the $\nabla\mu$p film library, which displays a comprehensive set of droplet morphologies. A detailed treatment of the full range of phenomena exhibited by this library will require extensive (and necessarily automated) analysis of the large number of OM images we collected. Results of this ongoing "data mining" analysis, including identification of the critical γ-contrast necessary to induce pattern-directed dewetting, will be reported in a future publication. This critical value is of interest because it represents the minimum chemical heterogeneity (e.g., defect or impurity) that can start film instability, and thus dewetting.

In conclusion, we present a method for fabricating a new type of surface specimen that exhibits a micropattern with a gradient in chemical contrast between the pattern domains. Our specimen includes design elements that enable the calibration of pattern chemical contrast through widely available techniques, such as contact angle measurements. Our specimen design is compatible with a variety of well-established routes for surface patterning of SAMs. In addition, with the aim of increasing the vigor and flexibility of SAM patterns, we illustrate a new method for patterning SAMs on silicon substrates that combines soft lithography, vapor deposition, and monochlorosilane chemistry, which produces monolayers resilient under a variety of conditions, for example, high-temperature annealing. This method provides reproducible, high-quality patterns on Si substrates in a way that enables multisample batch processing.

We demonstrated the value of $\nabla\mu$p specimens by employing them as reference substrates for surface-sensitive nanometrology and as a platform for producing libraries of thin film behavior. In the former case, we used a $\nabla\mu$p substrate to calibrate contrast in friction force AFM images with

respect to surface energy differences. The specimen was also useful in comparing the quality and effect of probe-functionalization. The specimen provides, within a single substrate, a spectrum of calibration relationships over a large range of conditions. Accordingly, we see $\nabla\mu$p specimens as a particularly useful new tool for advancing and understanding emerging SPM techniques. In later publications, we will employ these specimens toward advanced methods such as CFM and AFAM.

In the latter case, we applied $\nabla\mu$p specimens toward the high-throughput analysis of thin film stability. Our example specimen library encompasses a huge range of PS film dewetting behavior over the patterned area and flanking calibration fields. Automated optical microscopy (AOM) enabled rapid characterization of droplet morphology over the library. In this paper, we highlighted some of the interesting phenomena exhibited by the library. In particular, the $\nabla\mu$p provides insight into the effect of pattern chemical contrast, which was previously unexplored. In a later publication, we will report on the full range of phenomena exhibited in this library.

Acknowledgment. We acknowledge the NIST MSEL Director's Reserve Program and the NIST Advanced Technology Program for funding. Thanks to Alamgir Karim for useful discussions and to Donna Hurley (Materials Reliability Division, NIST) and Xiohong Gu (Building and Fire Research Laboratory, NIST) for providing feedback on our specimen designs. Thanks to Kimberly Briggman and Thomas Germer (Optical Technology Division, NIST) for assistance with ellipsometry and for lithographic masks, respectively.

Supporting Information Available: Fabrication details, including stamp preparation and notes on specimen lifetime, and detailed SPM procedures. This material is available free of charge via the Internet at http://pubs.acs.org.

References

(1) Huang, E.; Pruzinsky, S.; Russell, T. P.; Mays, J.; Hawker, C. J. *Macromolecules* **1999**, *32*, 5299−5303.
(2) Hoeppener, S.; Maoz, R.; Sagiv, J. *Nano Lett.* **2003**, *3*, 761−767.
(3) Maoz, R.; Frydman, E.; Cohen, S. R.; Sagiv, J. *Adv. Mater.* **2000**, *12*, 424−429.
(4) Bhushan, B.; Jun, Q. *Nanotechnology* **2003**, *14*, 886−895.
(5) Bhushan, B.; Xiaodong, L. *Int. Mater. Rev.* **2003**, *48*, 125−164.
(6) Whitesides, G. M.; Stroock, A. D. *Phys. Today* **2001**, *54*, 42−48.
(7) Reyes, D. R.; Iossifidis, D.; Auroux, P. A.; Manz, A. *Anal. Chem.* **2002**, *74*, 2623−2636.
(8) Sang Jin, L.; Il Woo, L.; Young Moo, L.; Hai Bang, L.; Gilson, K. *J. Biomater. Sci., Polym. Ed.* **2004**, *15*, 1003−1017.
(9) Turner, N. J.; Kielty, C. M.; Walker, M. G.; Canfield, A. E. *Biomaterials* **2004**, *25*, 5955−5964.
(10) Love, J. C.; Wolfe, D. B.; Jacobs, H. O.; Whitesides, G. M. *Langmuir* **2001**, *17*, 6005−6012.
(11) Xia, Y. N.; Whitesides, G. M. *Annu. Rev. Mater. Sci.* **1998**, *28*, 153−184.
(12) Heier, J.; Kramer, E. J.; Walheim, S.; Krausch, G. *Macromolecules* **1997**, *30*, 6610−6614.
(13) Kumar, A.; Biebuyck, H. A.; Whitesides, G. M. *Langmuir* **1994**, *10*, 1498−1511.
(14) Boltau, M.; Walheim, S.; Mlynek, J.; Krausch, G.; Steiner, U. *Nature* **1998**, *391*, 877−879.
(15) Karim, A.; Douglas, J. F.; Lee, B. P.; Glotzer, S. C.; Rogers, J. A.; Jackman, R. J.; Amis, E. J.; Whitesides, G. M. *Phys. Rev. E.* **1998**, *57*, R6273−R6276.
(16) Chaudhury, M. K.; Whitesides, G. M. *Science* **1992**, *256*, 1539−1541.
(17) Bhat, R. R.; Genzer, J.; Chaney, B. N.; Sugg, H. W.; Liebmann-Vinson, A. *Nanotechnology* **2003**, *14*, 1145−1152.
(18) Genzer, J.; Fischer, D. A.; Efimenko, K. *Appl. Phys. Lett.* **2003**, *82*, 266−268.
(19) Sehgal, A.; Ferreiro, V.; Douglas, J. F.; Amis, E. J.; Karim, A. *Langmuir* **2002**, *18*, 7041−7048.
(20) Ulman, A. *Thin Solid Films* **1996**, *273*, 48−53.
(21) Meredith, J. C.; Smith, A. P.; Karim, A.; Amis, E. J. *Macromolecules* **2000**, *33*, 9747−9756.
(22) Brinkmann, M.; Lipowsky, R. *J. Appl. Phys.* **2002**, *92*, 4296−4306.
(23) Smith, A. P.; Sehgal, A.; Douglas, J. F.; Karim, A.; Amis, E. J. *Macromol. Rapid Commun.* **2003**, *24*, 131−135.
(24) Roberson, S. V.; Fahey, A. J.; Sehgal, A.; Karim, A. *Appl. Surf. Sci.* **2002**, *200*, 150−164.
(25) Julthongpiput, D.; Fasolka, M. J.; Amis, E. J. *Microsc. Today* **2004**, *12*, 48−51.
(26) Xia, Y. N.; Whitesides, G. M. *Langmuir* **1997**, *13*, 2059−2067.
(27) Fadeev, A. Y.; McCarthy, T. J. *Langmuir* **2000**, *16*, 7268−7274.
(28) Fadeev, A. Y.; McCarthy, T. J. *Langmuir* **1999**, *15*, 7238−7243.
(29) Cao, C. T.; Fadeev, A. Y.; McCarthy, T. J. *Langmuir* **2001**, *17*, 757−761.
(30) Sugimura, H.; Hozumi, A.; Kameyama, T.; Takai, O. *Surf. Interface Anal.* **2002**, *34*, 550−554.
(31) Wu, S. *Polymer Interface and Adhesion*; Marcel Dekker: New York, 1982.
(32) Lenz, P.; Lipowsky, R. *Phys. Rev. Lett.* **1998**, *80*, 1920−1923.
(33) Girifalco, L. A.; Good, R. J. *J. Phys. Chem.* **1960**, *64*, 561.
(34) Frommer, J. *Angew. Chem., Int. Ed. Engl.* **1992**, *31*, 1298−1328.
(35) Tsukruk, V. V.; Bliznyuk, V. N.; Hazel, J.; Visser, D.; Everson, M. P. *Langmuir* **1996**, *12*, 4840−4849.
(36) Tsukruk, V. V.; Reneker, D. H. *Polymer* **1995**, *36*, 1791−1808.
(37) Brewer, N. J.; Leggett, G. J. *Langmuir* **2004**, *20*, 4109−4115.
(38) Reinstadtler, M.; Rabe, U.; Scherer, V.; Hartmann, U.; Goldade, A.; Bhushan, B.; Arnold, W. *Appl. Phys. Lett.* **2003**, *82*, 2604−2606.
(39) Kim, S.-W.; Sehgal, A.; Karim, A.; Fasolka, M. J. *Microsc. Today* **2003**, *11*, 30−32.
(40) Xie, R.; Karim, A.; Douglas, J. F.; Han, C. C.; Weiss, R. A. *Phys. Rev. Lett.* **1998**, *81*, 1251−1254.
(41) Ashley, K. M.; Meredith, J. C.; Amis, E.; Raghavan, D.; Karim, A. *Polymer* **2003**, *44*, 769−772.
(42) Luo, C.; Xing, R.; Zhang, Z.; Fu, J.; Han, Y. *J. Colloid Interface Sci.* **2004**, *269*, 158.
(43) Certain commercial equipment, instruments, or materials are identified in this document. Such identification does not imply recommendation or endorsement by the National Institute of Standards and Technology, nor does it imply that the products identified are necessarily the best available for this purpose.

NL050612N